CrossMark

Benefits of explicit urban parameterization in regional climate modeling to study climate and city interactions

M. Daniel[1] · Aude Lemonsu[1] · M. Déqué[1] · S. Somot[1] · A. Alias[1] · V. Masson[1]

Abstract

Most climate models do not explicitly model urban areas and at best describe them as rock covers. Nonetheless, the very high resolutions reached now by the regional climate models may justify and require a more realistic parameterization of surface exchanges between urban canopy and atmosphere. To quantify the potential impact of urbanization on the regional climate, and evaluate the benefits of a detailed urban canopy model compared with a simpler approach, a sensitivity study was carried out over France at a 12-km horizontal resolution with the ALADIN-Climate regional model for 1980–2009 time period. Different descriptions of land use and urban modeling were compared, corresponding to an explicit modeling of cities with the urban canopy model TEB, a conventional and simpler approach representing urban areas as rocks, and a vegetated experiment for which cities are replaced by natural covers. A general evaluation of ALADIN-Climate was first done, that showed an overestimation of the incoming solar radiation but satisfying results in terms of precipitation and near-surface temperatures. The sensitivity analysis then highlighted that urban areas had a significant impact on modeled near-surface temperature. A further analysis on a few large French cities indicated that over the 30 years of simulation they all induced a warming effect both at daytime and nighttime with values up to +1.5 °C for the city of Paris. The urban model also led to a regional warming extending beyond the urban areas boundaries. Finally, the comparison to temperature observations available for Paris area highlighted that the detailed urban canopy model improved the modeling of the urban heat island compared with a simpler approach.

Keywords Urban parameterization · Regional climate model · City and climate interactions · Urban heat island · ALADIN · TEB

1 Introduction

General circulation models (GCMs) are implemented at the global scale (Cubasch et al. 1992) to simulate and investigate long-term climatic evolutions. Dynamical downscaling (Giorgi 1990) approaches are now used in order to study specific regions of the globe by running higher resolution limited area models also called regional climate models (RCMs) that are driven by re-analyses or GCMs. Their horizontal resolutions of few tens kilometers make possible to more realistically model some physical or dynamical processes, and consequently to assess regional or local impacts of climate change as well as the potential feedback of surface heterogeneities on regional climate.

Surface characteristics of urban areas (imperviousness, thermal properties, three-dimensional geometry) alter radiative, energetic, turbulent, and hydrologic processes. They generate a specific local climate, especially positive anomalies in air temperature in the city compared to surrounding areas called urban heat island (UHI, Oke 1982). These urban effects interact with atmospheric boundary layer and local meteorology. Over long time periods, the urbanization dynamics mostly driven by demographic expansion leads to changes in land uses and land covers that may influence regional climate trends (Houghton et al. 2001). Based on observational time series over the second half of the twentieth century, warming effect due to urbanization were already observed at the regional scale in the United States (Stone 2007) and in China (Hua et al. 2008; Jones et al. 2008). Cities are consequently critical areas in that

✉ Aude Lemonsu
aude.lemonsu@meteo.fr

1   Météo-France/CNRS, National Center for Meteorological Resarch, 42 avenue Gaspard Coriolis, 31057 Toulouse cedex, France

the warming effects already observed there due to urban heat island could be amplified by the local effects of climate change. The scientific community in urban climate has a growing interest in these issues related to major societal challenges. This is less so in climate research community. To date, most climate models do not include explicit modeling of urban areas. Nonetheless, the spatial resolutions reached by some regional climate models (up to about 10 km or even less) may now justify and require a more realistic parameterization of surface exchanges between urban canopy and atmosphere.

Some regional climate studies investigated urban effects but with rather coarse resolution and simple slab representation of cities. Lamptey et al. (2005) studied the effects of land use changes due to urbanization and agriculture on regional climate of northeastern United States with a 36-km spatial resolution modeling configuration over 1990–1995 time period. McCarthy et al. (2012) simulated the climate evolution of United Kingdom between 1970–1990 and 2040–2060 running the HadRM3 model with a 25-km resolution.

Some studies favor a more realistic modeling of urban processes with specific urban models applied at one or few kilometers spatial resolutions that parameterize the complex radiative, energetic and turbulent interactions between the three-dimensional urban canopy and lower atmosphere. Früh et al. (2011) and Lemonsu et al. (2013) assessed this way the future climate of Frankfurt (Germany) and Paris (France) respectively, with offline simulations of urban climate forced by statistically or dynamically downscaled GCMs and RCMs. Nonetheless, the surface energy budget and turbulence generated by urban covers may impact the atmospheric characteristics, and these properties may be transported horizontally by advection. Inline atmospheric modeling coupled to urban model is required for explicitly taking into account feedback of cities on the atmosphere and potentially on regional climate. As an example, Yang et al. (2016) performed RCM simulations at 4-km resolution with the WRF atmospheric model over Phoenix area (AZ, US) to study impact of urbanization on precipitation. Using the same set-up over Tokyo (Japan), Kusaka et al. (2012) investigated evolution of heat stress for population, by comparing occurrences of August warm nights between 2080 and the present day. The computational time of these numerical studies that focus on specific cities with high spatial resolution significantly constrains the simulation duration. It is thus possible to study meteorological events or particular short time periods (e.g. specific seasons) of interest but impossible to investigate regional climate trends (e.g. climate trends over decades).

Trusilova et al. (2007) proposed an innovative and advanced approach by running the MM5 RCM (10-km resolution) coupled with the TEB urban canopy model (Masson 2000) over the Western Europe for July and December 2000–2005. Hamdi et al. (2014) run the ALARO model at 4-km resolution on a smaller domain over Belgium and north of France over the period 1960–1990, and compared TEB with a slab model for the 30 consecutive summers. Using TEB increases air temperature, which leads to a better representation of the nocturnal and diurnal urban heat islands.

Inspired by these works and those of McCarthy et al. (2012), the present study focuses on a regional climate modeling framework, by running ALADIN-Climate RCM over France with a 12-km spatial resolution and for a long-term simulation of 30 years. The objective is to evaluate the model performances for a past period for which observations are available. The sensitivity of the results to the representation of cities in the model is investigated, and especially the potential benefits that a complex urban canopy model can bring compared to a simpler representation. With this aim, three different parameterizations are compared: an experiment with vegetation only, an experiment with a simple parameterization describing cities as rock covers, and a last experiment including an urban canopy model. Section 2 is dedicated to the description of the ALADIN-Climate RCM model and of the simulation configurations, as well as the presentation of observations used for the model evaluation. After the general evaluation of the model in Sect. 3.1, Sect. 3.2 presents the result of the sensitivity study on precipitation and air temperature modeling over France domain. In Sect. 3.3, the impact of these experiments on the representation of the UHI for Paris area is investigated by comparison with long-term observations, and Sect. 4 presents the conclusions and perspectives of this study.

2 Method

2.1 Numerical modeling framework

2.1.1 ALADIN regional climate model

The atmosphere is here modeled by the ALADIN-Climate model (Aire Limitée Adaptation dynamique Développement InterNational) that is a bi-spectral, hydrostatic limited area regional climate model with a semi-Lagrangian advection and a semi-implicit scheme. ALADIN-Climate version 5 (Colin et al. 2010) has been widely used in the CORDEX initiative over the Med-CORDEX, Euro-CORDEX and CORDEX Africa domains (Tramblay et al. 2013; Jacob et al. 2014; Nabat et al. 2014, 2015; Bador et al. 2017; Kjellström et al. 2017; Nikulin et al. 2018). In this study, we apply for the first time the most recent version of ALADIN-Climate, that is to say its version 6. The dynamical core is based on the cycle 37t1 of ARPEGE-IFS and the physical package

has been largely renewed since version 5. In particular, it includes a new turbulence scheme with a 1.5-order prognostic scheme for the turbulence kinetic energy (Cuxart et al. 2000); a new convection scheme including dry, shallow, and deep convection (Piriou et al. 2007; Guérémy 2011); a new large-scale microphysics scheme with prognostic liquid/solid cloud/rain variables based on the work of Lopez (2002) and a new radiative scheme for infrared radiation (RRTM, Rapid Radiative Transfer Model, Mlawer et al. 1997). An updated version (6 bands) of the shortwave radiation scheme is used (Fouquart and Bonnel 1980; Morcrette et al. 2008). Similarly to the version 5, the mixing length is nonlocal and based on Bougeault and Lacarrere (1989) and the PDF-based cloud scheme is based on Ricard and Royer (1993). Note that ALADIN-Climate version 6 shares the same dynamical core, atmosphere physical package and land-surface module as their general circulation model counterparts in ARPEGE-Climate version 6 or CNRM-CM6, that are currently used to run the CMIP6 experiments (e.g. Watson et al. 2017; Abdel-Lathif et al. 2018).

2.1.2 SURFEX land surface modeling system

Contrary to version 5, ALADIN-Climate v6 is now run together with the SURFEX v8 land surface modeling platform (Masson et al. 2013), which uses a tile approach to simulate surface fluxes and properties over natural land surface, town, lake, and sea areas. This version of SURFEX is similar to the version used in the CNRM-CM5 global climate model (Voldoire et al. 2013). Turbulent fluxes over seas and oceans and over inland waters are both computed from the bulk aerodynamic equations, using an exchange coefficient and a surface roughness length. These are computed by the ECUME (Exchange Coefficients from Unified Multi-campaigns Estimates) iterative approach (Belamari and Pirani 2007) for seas and oceans. For inland waters, the roughness length comes from Charnock equation (1955). In both cases, a water surface temperature is prescribed from the temporal binomial interpolation of monthly ERAinterim data. The land surface is represented via the Interaction Soil-Biosphere-Atmosphere (ISBA) model (Noilhan and Mahfouf 1996). ISBA is a relatively simple land surface model that uses the force-restore method to calculate the time evolution of the surface energy and water budgets. It includes a comprehensive sub-grid hydrology to account for the heterogeneity of precipitation, topography and vegetation in each grid cell (Decharme and Douville 2006). In-depth evaluation of this model can be found in Decharme and Douville (2007) and Alkama et al. (2010).

Depending on the chosen modeling configuration, it is possible to deal explicitly with urban covers using the Town Energy Balance (TEB, Masson 2000) model that is implemented in SURFEX. Contrary to the simple slab approach

that considers urban covers are simple plane surfaces, TEB describes the urban canopy by the approach of mean urban canyon (Oke 1987). It is composed of elementary surfaces (roof, road, walls) and defined with mean geometric parameters (building density, building height, and street aspect ratio) and mean thermal and radiative properties. With this relative simple geometry, TEB is able to simulate shadow effects, shortwave and longwave radiative trapping and reflections within the canyon, and to compute for each surface the radiative budget for shortwave and longwave radiation, and the energy budget, i.e. sensible heat (H), latent heat (LE), and heat storage (G) fluxes. Air temperature and specific humidity are computed inside the canyon at mid-height of buildings, based on turbulent exchanges between the canyon facets, the air volume inside the canyon, and the atmosphere above.

Eventually, SURFEX computes mean contributions of the surface, by averaging the contributions from each type of covers (or tile) according to their corresponding cover fraction. It provides the surface boundary conditions for ALADIN, i.e. upgoing radiation, latent and sensible heat fluxes, and momentum flux, as well as the composite surface albedo that is required for the radiative scheme.

2.1.3 Simulation configuration

The simulation configuration used here follows the CORDEX protocol for the so-called "evaluation" run (Giorgi et al. 2009). In this study, ALADIN-Climate covers a small domain (180×180 grid points) centered over the France metropolitan area (see Fig. 1) with a 12-km grid mesh. It uses a Lambert conformal projection centered at 2°E, 47°N, a 11-points bi-periodization zone, a 2×8-points relaxation zone, 91 vertical levels, and a 450-s timestep. The domain has been chosen large enough to cover a part of Western Europe and therefore to ensure a adequate spatial spin-up (Leduc and Laprise 2009) and avoid any influence of lateral boundary conditions on the study area (France). The simulation is performed for the 1980–2009 time period for which lateral boundary conditions and sea surface temperatures are provided by the ERAinterim reanalyses (Dee et al. 2011). The atmospheric and surface variables are initialized from ERAinterim and a 1-year spin-up integration is carried out to discard the drifting period, in particular for soil moisture.

In addition to lateral and surface boundary conditions, the ALADIN-Climate simulation is also driven by evolving greenhouse gas concentrations (CO_2, CH_4, N_2O, CFC-11, CFC-12, ozone) following CMIP5 recommendations and evolving aerosols using the dataset developed by Nabat et al. (2013). Note that these external forcings come from observations and are not constant with time. The aerosol forcing prescribed in ALADIN-Climate is a recently-developed dataset covering the Euro-Mediterranean area (Nabat et al.
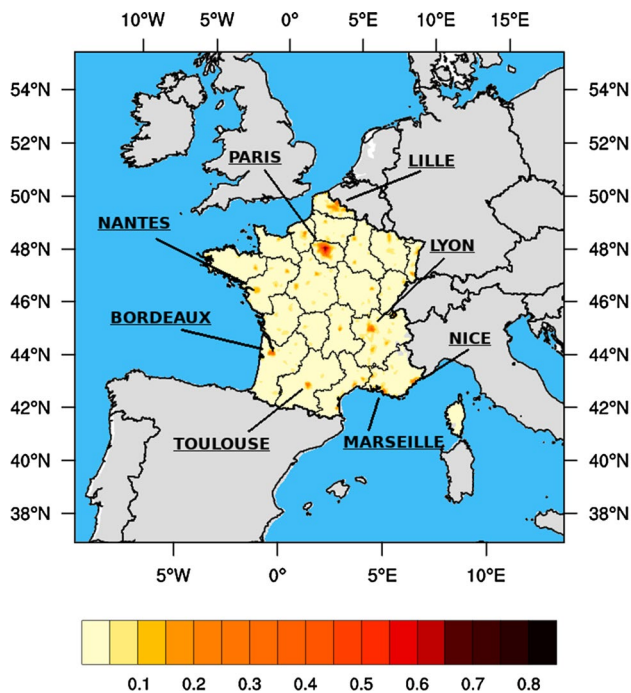
	City	Population[a] (hab)	Area (km^2)	Urbanization (%)
1	Paris	10 659 489	2 845	63
2	Lyon	1 620 331	1 181	46
3	Marseille	1 578 484	1 732	15
4	Lille	1 037 939	442	30
5	Nice	944 022	744	18
6	Toulouse	935 440	812	34
7	Bordeaux	889 543	1 172	41
8	Nantes	622 693	538	14

For each city population and surface area are indicated for the whole urban area (including adjacent municipalities). The urbanization rate is, for the city center, the fraction of impervious urban covers in the corresponding cell of ALADIN-Climate 12-km resolution grid

[a] 2014 census data

Fig. 1 ALADIN-Climate simulation domain on which are indicated the location of the French eight largest cities. Color gradations shows the impervious surface fraction

2013) with a spatial and temporal variability for 5 different aerosol classes (sulfate, organic carbon, black carbon, desert dust, sea salt). For each of the classes, the dataset is constituted by 12 maps of AOD (1 per month) plus a spatially-homogeneous vertical profile. In addition, for the sulfate aerosols, a trend is applied over the period to take into account the brightening effect. The added-value of using this new dataset in ALADIN-Climate was shown by Nabat et al. (2014, 2015).

The surface information are defined from the Ecoclimap II database (Faroux et al. 2013) which provides for Europe a 1-km resolution land cover classification including 273 covers, and associated ecosystems and surface parameters. Based on the Corine Land Cover map over Europe (EEA 2005), it is a static classification representative of year 2000 and there is no land covers modification over the simulation period. The Ecoclimap II is projected on ALADIN-Climate simulation grid, so that each mesh consists in a combination of land covers. The fractions of sea, inland water, natural land surface and urban areas are derived from these information. As illustration, impervious fraction map over France is shown in Fig. 1, with the corresponding values for the French eight largest cities in Table 1. Most of input data required by the surface models are also defined from Ecoclimap II. For TEB, geometric parameters and material properties are assigned to each

urban cover. For ISBA, Ecoclimap II provides the vegetation specifications, e.g. vegetation fraction, leaf area index, albedo, emissivity. In addition, the soil texture characteristics (sand and clay fractions), used to compute hydrological and thermal soil properties, are given here by the harmonized world soil database (HWSD, Batjes 2009).

2.1.4 Description of urban areas for sensitivity study

The regular configuration of ALADIN-Climate model does not model explicitly urban processes. Urban areas are described as rock covers with high roughness (Colin et al. 2010) to approach in a simple way thermal, radiative, and imperviousness properties of built-up surfaces, and they are modeled with ISBA. The coupling of SURFEX to ALADIN-Climate makes now possible to activate the TEB urban canopy model in the regional climate simulations, which was not the case with previous versions.

For the present study, the objective is twofold: first, to evaluate the potential impact of urbanization on the regional climate; second, to assess the possible benefits of a detailed urban canopy model compared to the simpler approach currently applied in ALADIN-Climate. With this aim, three experiments with different descriptions of land uses and land covers for urban areas are compared: (1) CITY experiment corresponding to the explicit description and modeling of cities with TEB, (2) ROCK experiment that is the conventional approach of ALADIN-Climate for which impervious covers are replaced by rocks and computed with ISBA, and (3) VEG experiment for which cities are replaced by the surrounding natural covers (comparable to the case studied by Trusilova et al. 2007) and also modeled with ISBA. Depending on the experiment,

the land cover data come from an adaptation of ECOCLI-MAPII database as described in "Appendix 1".

2.2 Observational data

2.2.1 SAFRAN analyses

ALADIN-Climate in its last version has not been deeply evaluated yet. A first stage of general evaluation of its default configuration is conducted and presented hereafter for the France domain. The observational data are the SAFRAN analyses (Durand et al. 1993, 1999). They are gridded surface meteorological data over France with a regular grid of 8-km horizontal resolution covering the 1960–2010 time period. They include 2-m air temperature (hourly timestep), liquid and solid precipitation rate (daily), incoming solar radiation (hourly), as well as 2-m relative humidity, cloudiness, and 10-m wind speed (that are not used here for the evaluation).

These data have been evaluated by Quintana-Segui et al. (2008) and Vidal et al. (2010) by comparison with the Aurelhy climatology based on a statistical mapping method (Bénichou and Le Breton 1987) for precipitation and temperature, and with surface stations for temperature and radiation. Both highlighted the quality of the precipitation rate and the near-surface air temperature despite an overestimation of T_{min} by $+ 1.0$ °C in winter and $+1.5$ °C in summer and an underestimation of T_{max} by $- 1.1$ °C in winter and $- 1.6$ °C in summer. However, Vidal et al. (2010) found an underestimation of $- 6$ to $- 10$ W m^{-2} of the incoming solar radiation.

2.2.2 Temperature observation time series for Paris region

For a specific analysis of urban climate over Paris area (presented in Sect. 3.3), homogenized long-term time series covering the simulation period 1980–2009, and coming from three Météo-France stations and based on the PRODIGE method (Mestre et al. 2013). The first station is located in the Montsouris public park in Paris city center (referred to as Montsouris) and used as urban reference to characterize the urban temperature (T_{urb}). The other two stations are used as rural reference stations. They are located in the Paris surrounding municipalities of Chartres (southwest of Paris) and Melun (southeast of Paris) in natural environments. The rural areas temperature (T_{rur}) is computed as the average of both Chartres and Melun stations temperatures. The urban heat island can be computed as the temperature difference UHI = $T_{urb} - T_{rur}$.

For comparison between model results and observations, modeling data are extracted at the closest 12-km resolution grid cell to station locations. Table 2 presents for each experiment (VEG, ROCK and CITY) the land use covers for grid cells corresponding to the three stations. For Chartres and Melun stations, the grid cells are composed of around 90% of natural covers (mostly crops (55%) with broadleaf trees and grassland), for which 47% of bare soil for Melun and 39% for Chartres. Fractions are quite comparable in all experiments for these stations. For Montsouris station, the corresponding grid cell for CITY configuration includes 63% of impervious areas (21% of building and 42% of road), 9% of vegetation and 28% of bare soil (see Table 2). The mean building height reaches 17 m with a canyon aspect ratio (ratio of building height to distance between buildings) of 0.36, a wall surface density of 0.48 m^2 m^{-2}, and a roughness length of 1.54 m. In case of ROCK, the cell is composed of 63% of rocks, 28% of bare soil, and 9% of vegetation only, whereas for VEG the conversion of urban areas in natural covers leads to 76% of bare soil and 24% of vegetation.

3 Results and discussion

3.1 Evaluation of ALADIN-climate default configuration

Model outputs are compared to SAFRAN analyses of daily precipitation rates, incoming solar radiation, and daily minimum (T_{min}) and maximum (T_{max}) near-surface temperatures at seasonal scale over the 1980–2009 time period. For this, SAFRAN analyses data have been interpolated on the ALADIN-Climate grid, and 2-m temperature fields have been adjusted for topography differences

Table 2 Land use fractions given as fraction of the total grid cell

	Montsouris			Chartres			Melun		
	VEG	ROCK	CITY	VEG	ROCK	CITY	VEG	ROCK	CITY
Building fraction	/	/	0.21	/	/	0.03	/	/	0.04
Road fraction	/	/	0.42	/	/	0.07	/	/	0.07
Rock fraction	0.00	0.63	0.00	0.00	0.10	0.00	0.00	0.11	0.00
Vegetation fraction	0.24	0.09	0.09	0.57	0.51	0.51	0.47	0.42	0.42
Bare soil fraction	0.76	0.28	0.28	0.43	0.39	0.39	0.53	0.47	0.47

between SAFRAN and ALADIN-Climate by applying an adiabatic gradient.

3.1.1 Daily precipitation rate

Modeled and observed precipitations rates are compared at seasonal scale. They are globally overestimated by ALADIN-Climate in winter and spring with mean biases of $+0.23$ and $+0.40$ mm day^{-1}, respectively (Table 3), and underestimated in summer and autumn with mean biases of -0.41 and -0.07 mm day^{-1}. These biases are within the range of model from the Euro-CORDEX project and the works of Prein et al. (2015), that computed for different RCMs (at a 12-km resolution) the mean biases over the France domain. They found values ranging between -0.25 and $+0.60$ mm day^{-1} for winter (DJF) and -0.60 and $+0.70$ mm day^{-1} for summer (JJA).

Figure 2a, b presents the maps of difference in mean daily precipitation rates between ALADIN-Climate and SAFRAN for DJF and JJA. For both seasons, the biases do not exceed ± 0.5 mm day^{-1} for most of France. A spatial variability of biases is nonetheless noted: precipitation rates are overestimated in winter by 4 mm day^{-1} in localized mountainous regions (Alps, Pyrenees, Massif Central), and underestimated in summer by -0.5 to -1 mm day^{-1} in the southern half of France. As presented in Fig. 2c, it is intesting to emphasize that the inter-annual seasonal variability

of precipitation rates (averaged over France) is in adequacy with SAFRAN data for both seasons with temporal correlation coefficient of 0.86 in summer and 0.98 in winter. The ALADIN-Climate precipitation rate seem however to indicate a drying trend with time that is not observed with SAFRAN analyses. This could be explained by a brightening effect in the model i.e. by a decrease in aerosol optical depth leading to an increase in incoming shortwave radiation (see next section), then an increase in surface temperature, a decrease in evaporation and finally a decrease in precipitation.

3.1.2 Incoming solar radiation

The main defect of ALADIN-Climate simulations is the under-representation of cloud cover that translates in a strong overestimation of the incoming solar radiation all over France and whatever the season (see Fig. 3a, b). The comparison between ALADIN-Climate and SAFRAN of the year-by-year evolution of incoming solar radiation, averaged over France for DJF and JJA (Fig. 3c, d), shows a positive bias of $+12.7$ W m^{-2} in winter, that strengthens in summer up to $+40.7$ W m^{-2}. For JJA, one can note that Hamdi et al. (2012) found a similar bias with a former version of ALADIN-Climate that was also attributed to the under-representation of cloud cover.

Table 3 Seasonal biases (and correlation coefficient in brackets for DJF and JJA) of ALADIN-SURFEX compared to SAFRAN averaged over the French metropolitan area

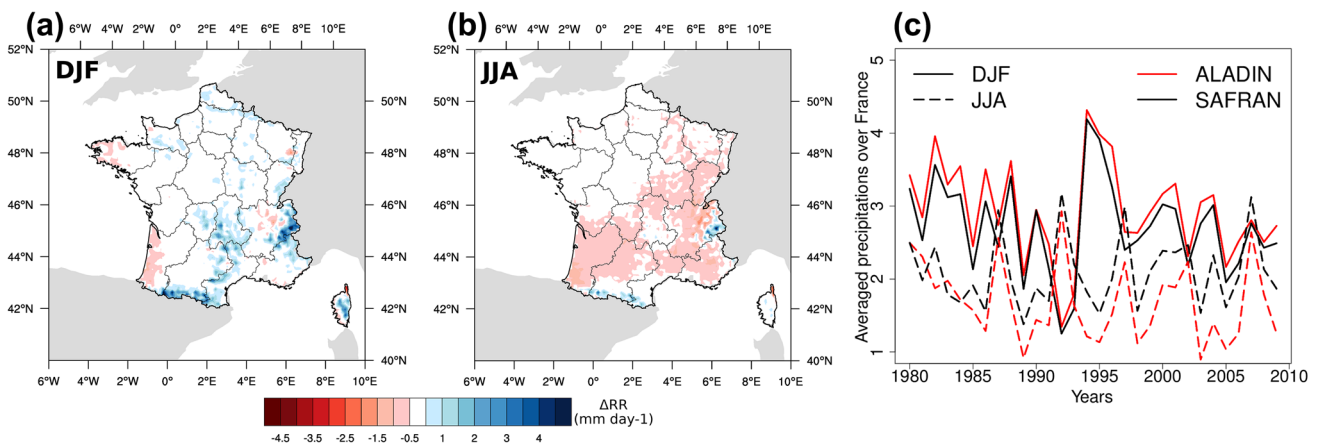| Seasons	DJF	MAM	JJA	SON
Precipitation rate (mm day^{-1})	$+0.23$ (0.98)	$+0.40$	-0.41 (0.86)	-0.07
Incoming solar radiation (W m^{-2})	$+12.7$ (0.82)	$+34.0$	$+40.7$ (0.91)	$+23.1$
T_{min} (°C)	-1.12 (0.99)	-1.13	$+0.09$ (0.96)	-0.21
T_{max} (°C)	$+0.64$ (0.97)	$+0.42$	$+2.79$ (0.98)	$+1.31$

Fig. 2 ALADIN-Climate biases relative to SAFRAN (**a, b**) and temporal evolutions (**c**) of precipitation rates (in mm day^{-1}) for DJF and JJA
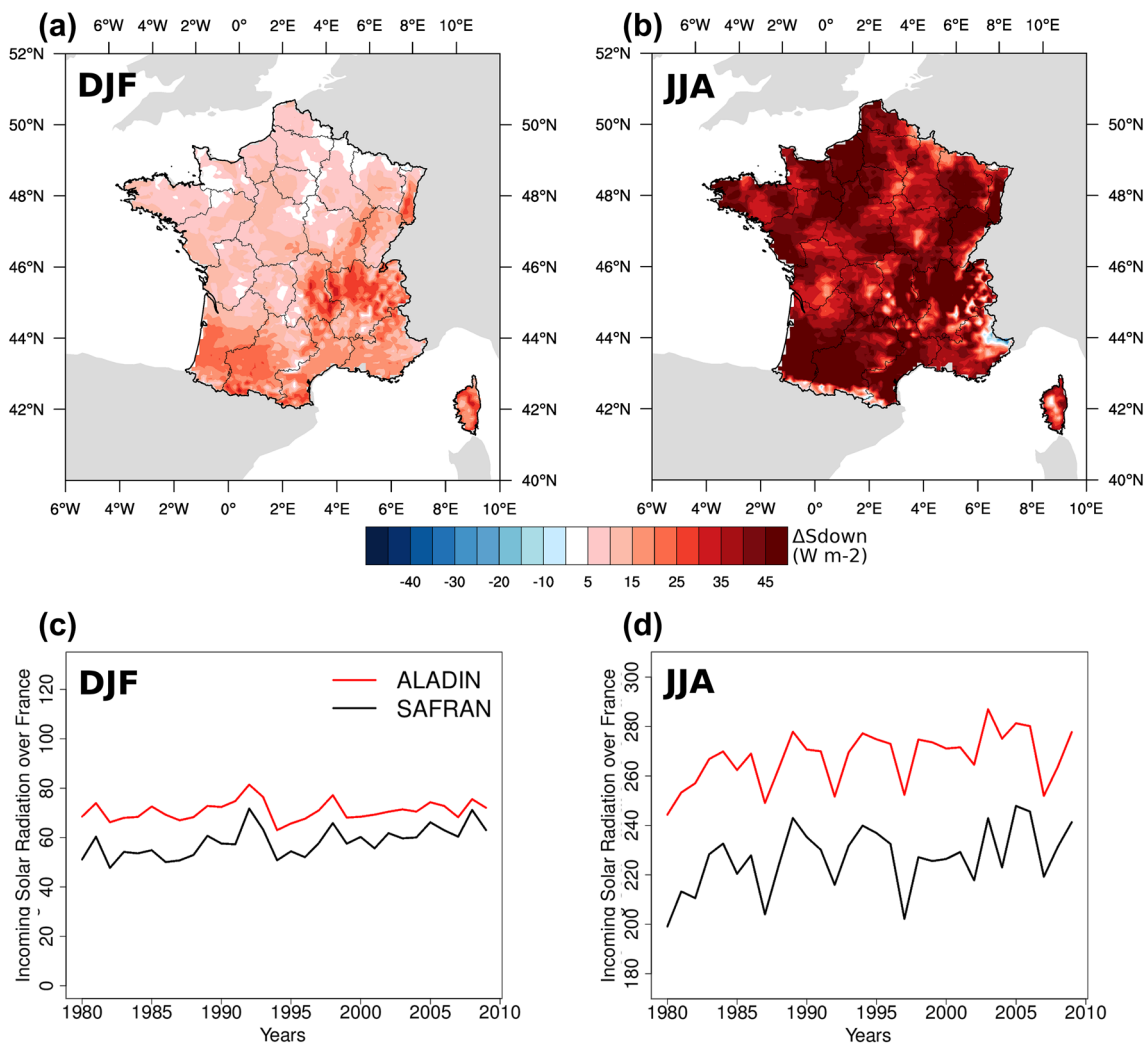
Fig. 3 ALADIN-Climate biases relative to SAFRAN and temporal evolutions (in W m^{-2}) of the incoming solar radiation for DJF and JJA

As summarized in Table 3, this strong positive bias is also noticed for transition seasons. It should be recalled however that SAFRAN analysis data underestimate the incoming solar radiation by -6 to -10 W m^{-2} compared to surface weather stations data (Vidal et al. 2010), so that ALADIN-Climate biases are likely less than the values presented in Table 3.

Although the incoming solar radiation suffers from a strong overestimation in the model, the inter-annual seasonal variability is well represented. In particular, the comparison between model and SAFRAN analyses (Fig. 3c, d) indicates a good correlation between the positive peaks for 1992 and 1998 winters, and for the 2003 heatwave, as well as between the negatives peaks for 1987, 1992, 1997 and 2007 summers. Temporal correlation coefficients reach 0.82 in winter and 0.91 in summer.

In addition, ALADIN-Climate reproduces the increase with years in incoming solar radiation that is observed and related to sulfate load decrease in Europe since the 1980s (Nabat et al. 2014).

3.1.3 Minimum and maximum daily temperature

Modeled and observed minimum daily temperatures are compared, based on difference maps in T_{min} between ALADIN-Climate and SAFRAN averaged seasonally over the 30-years period (Fig. 4a, b), and by comparing the year-by-year evolution of the seasonal T_{min} averaged over France (Fig. 4c, d). The same is done for T_{max} (Fig. 5).

T_{min} is relatively well simulated in JJA with a mean bias of $+0.1$ °C. However, this bias is likely to be greater since T_{min} provided by SAFRAN analyses can be overestimated by
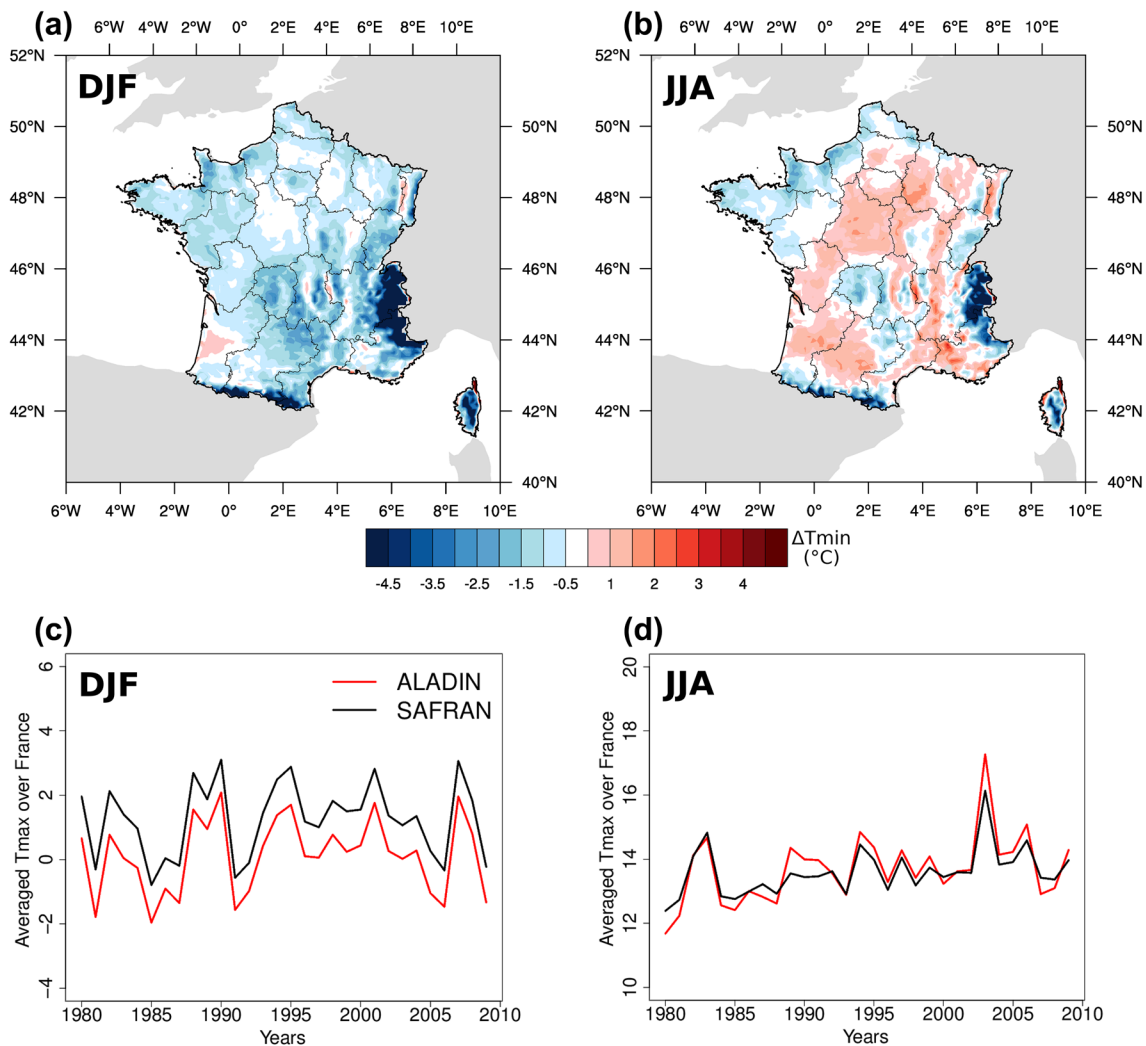
Fig. 4 ALADIN-Climate biases relative to SAFRAN and temporal evolutions (in °C) of T_{min} for DJF and JJA

+1 °C as mentioned in Sect. 2.2.1. On the contrary, the T_{min} underestimation by the model for other seasons by −0.2 °C in SON and −1.1 °C in DJF and MAM (see Table 3) can be partly explained by this defect of SAFRAN T_{min} analyses. Nonetheless a cold bias exceeding locally 4 °C is noted over mountainous regions. It was also observed by Vautard et al. (2013) and attributed to the too conservative ground snow scheme in ISBA, i.e. the snow scheme allows to maintain snow even when surface temperatures are above 0 °C which may not be always appropriate.

On the contrary, T_{max} is warmer in ALADIN-Climate simulation than in SAFRAN analyses for all seasons (see Fig. 5; Table 3) with biases between +0.4 °C in MAM and +2.8 °C in JJA. This is partially explained by the underestimation of T_{max} in SAFRAN analyses (Sect. 2.1.1), but also by a feedback of the incoming solar radiation overestimation (Sect. 3.1.2). Even though the model biases cannot be neglected, they are considered reasonable in regard with

past studies that have shown mean biases between −3 °C and +3 °C over Europe (Christensen et al. 2008; Vautard et al. 2013).

In consistency with precipitation rate and incoming solar radiation, the inter-annual seasonal variability of T_{min} (correlation of 0.99 in DJF and 0.96 in JJA) and T_{max} (correlation of 0.97 in DJF and 0.98 in JJA) is in agreement with SAFRAN analyses. For example, cold waves in 1985, 1987, 1991 and 2006 can be highlighted on Figs. 4c and 5c while 2003 and 2005 heatwaves are well represented in Figs. 4d and 5d.

3.2 Impact of the urban modeling at the regional scale

The general evaluation of ALADIN-Climate v6 simulations presented in previous section indicates the model performs correctly despite a warm bias in summer T_{max}. It is
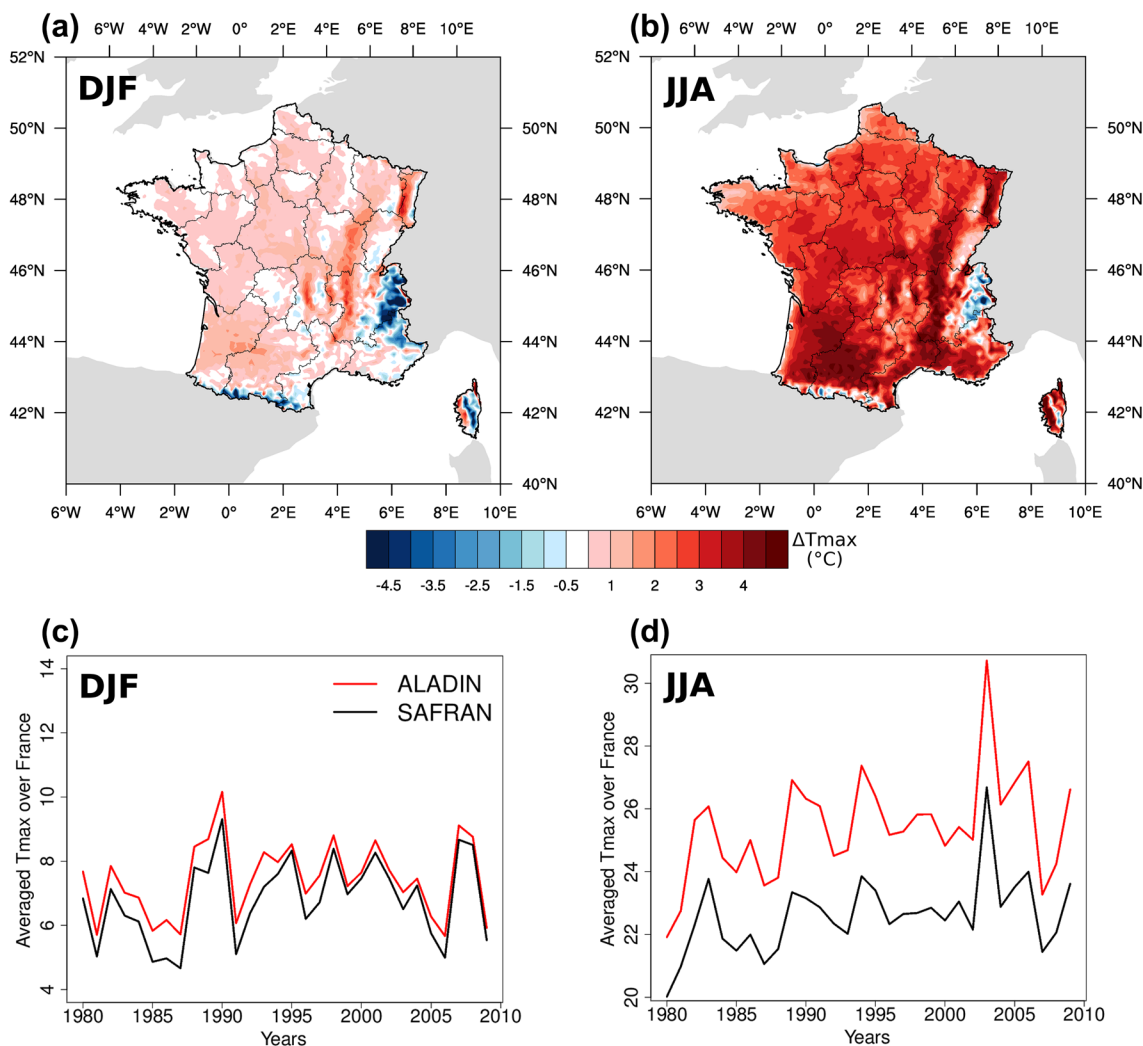
Fig. 5 ALADIN-Climate biases relative to SAFRAN and temporal evolutions (in °C) of T_{max} for DJF and JJA

consequently possible to assess the impact of the land use representation and associated surface parameterizations from the three sensitivity experiments presented in Sect. 2.1.4 and "Appendix 1". To compare the urban effects simulated with ROCK or CITY, the VEG experiment is taken as reference. The maps of significant differences ROCK minus VEG and CITY minus VEG are presented and discussed for the precipitation rate, T_{min}, and T_{max}. Since the three simulations are driven by the same large scale atmospheric conditions and are not independant, the significance threshold (here defined at 95%) is based on a Student test carried out on the series of differences.

3.2.1 Daily precipitation rate

The differences in daily precipitation rates computed for DJF between ROCK and VEG (Fig. 6a) show there is no impact on precipitation intensities. The CITY experiment

seems to weakly increase the precipitations over the cities of Paris and Bordeaux and slightly reduce them over the northwest of France (Fig. 6b). However the signal is not clear and the values ranging between -0.1 and $+0.1$ mm day^{-1} are likely linked to the chosen significance threshold. Similar behaviors have been observed for the other three seasons (not shown here).

3.2.2 Minimum and maximum daily temperature

The differences in T_{min} (T_{max}) between ROCK and VEG and between TEB and VEG are presented as maps in Fig. 7 (in Fig. 8). Note that for these maps, the differences less than -0.1 °C, although they might be statistically significant, are neglected (colored in white) because they remain very low in a physical sense and with respect to the temperature measurement precision.
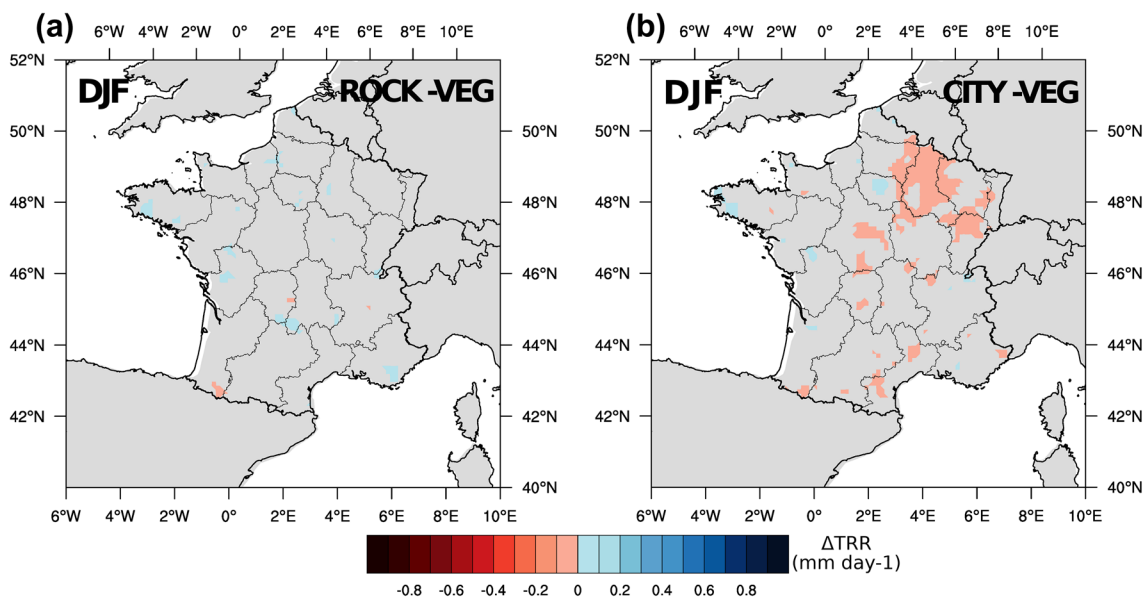
Fig. 6 Differences of precipitation rates (in mm day^{-1}) for DJF between ROCK and VEG (**a**) and between CITY and VEG (**b**)

Regarding impacts on near-surface temperatures, Fig. 7 shows that ROCK results in an increase in T_{min} compared to VEG. The heat capacity of rocks favors heat storage during the day and limits the nocturnal cooling of surface and low atmosphere. Seasonal differences are noticed. In JJA, the storage is exacerbated by stronger incoming solar radiation, and differences in T_{min} are therefore higher than in DJF (see Fig. 7). The T_{min} anomalies are maximum for urbanized grid points where surface properties directly influence air temperature above. The values obtained for grid points corresponding to the French eight largest cities are presented in Table 4. The T_{min} anomaly between ROCK and VEG is maximum for the city of Paris. It reaches $+1.3$ °C in JJA and $+0.5$ °C in DJF.

The urban warming effect on T_{min} extends beyond the physical boundaries of urban areas that highlights a regional impact. This effect is here quantified based on the Regional Index Coefficient (REI). This coefficient was proposed by Trusilova et al. (2007) in a similar study performed over western Europe with the COSMO RCM for comparison of a simulation with the TEB urban canopy model and a simulation with only vegetation. It is expressed as:

$$REI(x) = \frac{A_{rur_{aff}}(x) + A_{urb}}{A_{urb}}$$

where x is T_{min} (or T_{max}), A_{urb} the urban area defined as the number of grid cells with urban fraction greater or equal to 10%, and $A_{rur_{aff}}(x)$ the non urban area (i.e. cells where urban fraction is less than 10%) affected by a significant

temperature difference between the two simulations ROCK and VEG (or CITY and VEG). In this study, the significance is defined by a Student test carried out on the VEG experiment and with a threshold value set at 90%. The REI coefficient is by construction greater or equal to 1. During summer, the REI is 1.17 which reveals that ROCK significantly impacts a domain 17% larger than the urban areas. In winter, the REI is 1 that means urban effects do not extend spatially.

A seasonal variability is also noticed for T_{max} with a cooling effect in DJF when comparing ROCK and VEG, and a warming effect in JJA. In DJF, the cooling of near-surface temperature is emphasized in ROCK probably due to the higher roughness length defined in ROCK than in VEG that favors the evaporation of available water by turbulent mixing (Fig. 8a; Table 4). Inversely in JJA, the low precipitation rate should result in a reduction of evaporation and an increase in sensible heat flux that slightly warms the near surface temperature (see Fig. 8c; Table 4). In addition, although Fig. 8 shows a wide domain of influence (especially in summer), the REI value of 1 (Table 5) does not translate any regional impact of the cities. It should be noted that these differences between anomalies maps presented in Figs. 7 and 8, and the REI calculated according to Trusilova et al. (2007), are related to the choice in threshold values and significance test. This point is discussed in "Appendix 2".

For the CITY experiment, the two-dimensions canyon approach of the TEB urban model results in a temperature increase compared to VEG but also to ROCK that is explained by two processes. First the canyon geometry leads
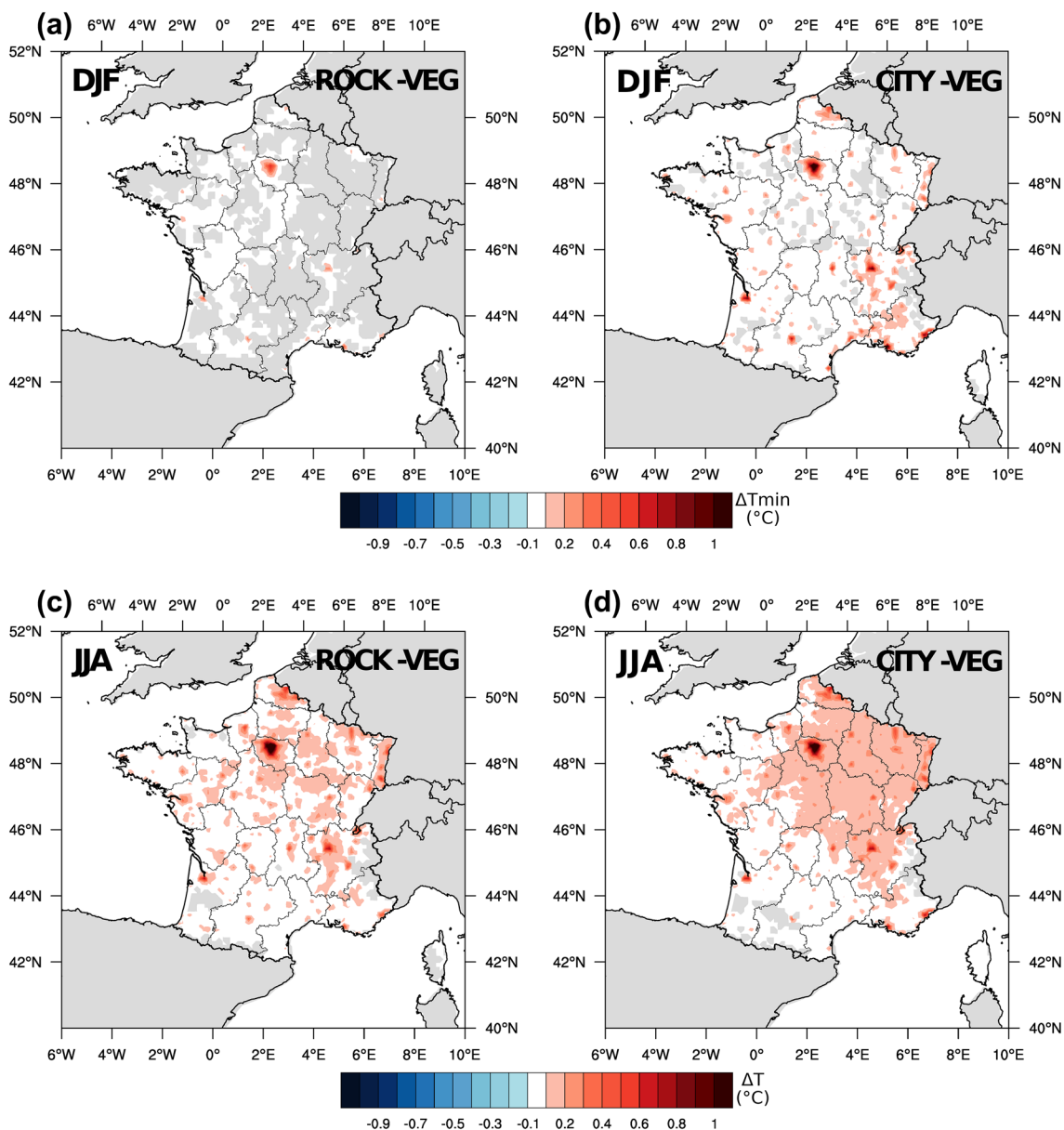
Fig. 7 Differences of T_{min} (in °C) for DJF (top) and JJA (bottom) between ROCK and VEG (**a, c**) and between CITY and VEG (**b, d**)

to multiple reflections of incoming solar radiation inside the street during the day that increase energy absorption by urban facets, and it prevents the cooling at night by trapping infrared radiation emitted by urban facets. Second, the canyon shape increases the exchange surface density between air and road and walls, which results in an amplification of storage and sensible heat fluxes.

The T_{min} anomalies calculated between CITY and VEG are greater than for ROCK both in winter and summer (Fig. 7b, d). They reach at maximum 1.1 and 1.5 °C in DJF and JJA, respectively for Paris grid point (Table 4). The spatial domain influenced by cities is also larger in CITY than

in ROCK, covering 8% in DJF and 29% in JJA of non-urban areas. One can note that Trusilova et al. (2007) also found a larger impact in summer than in winter, but with lower extensions (6% only in summer).

Positive anomalies in T_{max} are obtained between CITY and VEG whatever the season, and are greater than that calculated between ROCK and VEG, up to 0.72 and 1.31 °C in DJF and JJA, respectively, for Paris (Fig. 8b, d; Table 4). The spatial domain influenced by the cities is however limited in DJF (REI of 1.03) whereas it reaches 17% in JJA (Table 5). Note that in comparison, Trusilova et al. (2007) found a domain of influence of 28%.
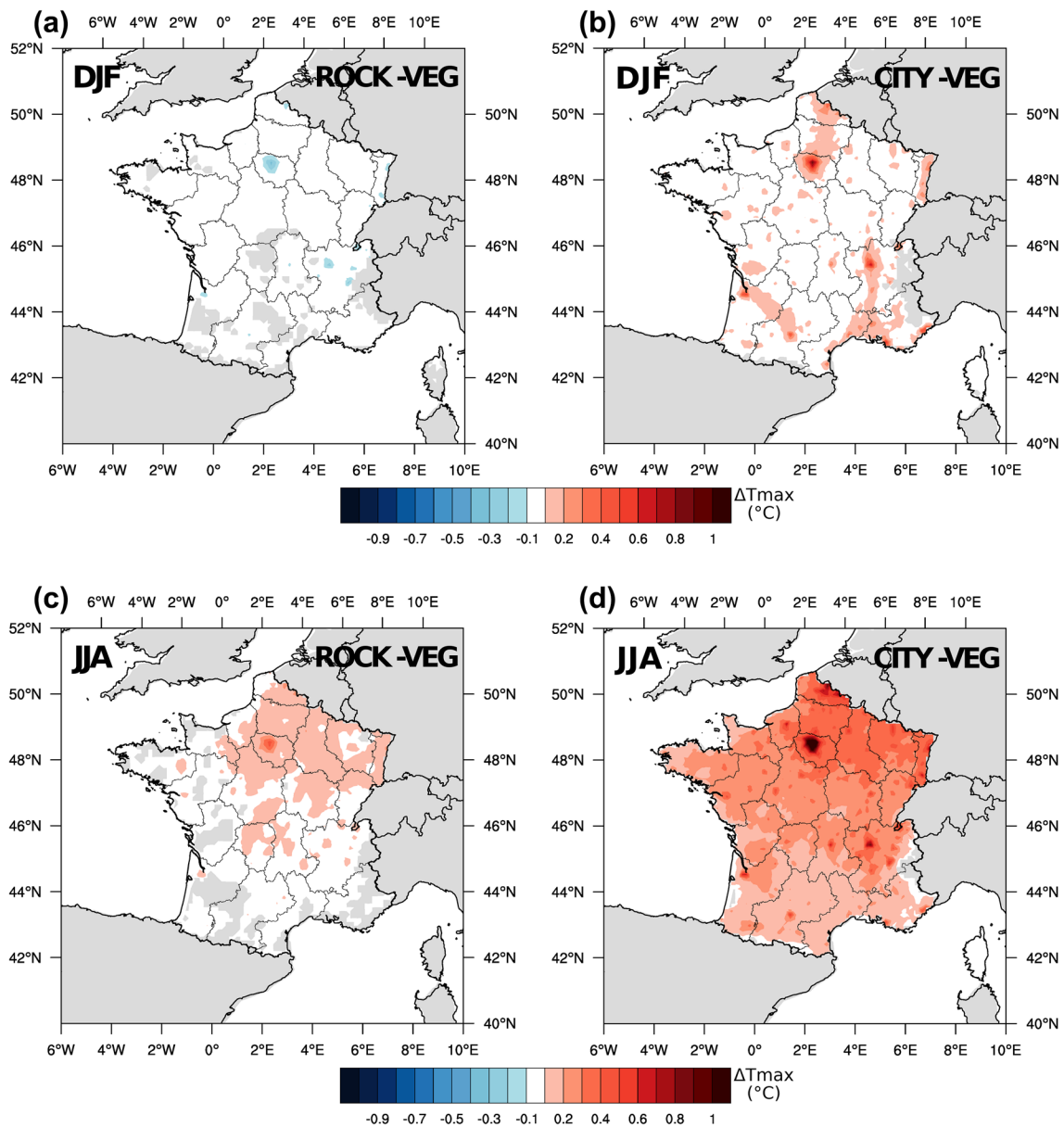
Fig. 8 Differences of T_{max} (in °C) for DJF (top) and JJA (bottom) between ROCK and VEG (**a, c**) and between CITY and VEG (**b, d**)

Table 4 Anomalies (in °C) of T_{min} and T_{max} between the ROCK (left) or the CITY (right) experiments and VEG for the French largest cities

| | ROCK vs VEG | | | | CITY vs VEG | | | |
| | DJF | | JJA | | DJF | | JJA | |
	ΔT_{min}	ΔT_{max}	ΔT_{min}	ΔT_{max}	ΔT_{min}	ΔT_{max}	ΔT_{min}	ΔT_{max}
Paris	0.49	−0.30	1.32	0.42	1.13	0.72	1.47	1.31
Lyon	0.25	−0.25	0.74	0.20	0.97	0.69	0.75	0.84
Marseille	0.13	−0.02	0.12	0.00	0.41	0.29	0.23	0.20
Lille	0.38	−0.18	0.74	0.16	0.91	0.52	0.70	0.62
Nice	0.12	−0.07	0.27	−0.01	0.64	0.37	0.45	0.24
Toulouse	0.30	−0.13	0.35	0.10	0.74	0.45	0.37	0.53
Bordeaux	0.11	−0.12	0.59	0.23	0.42	0.33	0.62	0.82
Nantes	0.10	−0.06	0.28	0.10	0.24	0.17	0.26	0.41

Table 5 Regional Effect Index computed between the ROCK (left) or the CITY (right) experiments and VEG using the Student test with a 90% threshold

	ROCK vs VEG		CITY vs VEG	
	DJF	JJA	DJF	JJA
T_{min}	1.00	1.17	1.08	1.29
T_{max}	1.00	1.00	1.03	1.17

It was shown in this section that the urban areas have an impact on modeling near-surface temperature over France domain even for a spatial resolution of 12 km. A general warming is noticed using the standard approach applied in ALADIN-Climate for cities (ROCK). It is amplified when cities are explicitly described and modeled using the TEB urban canopy parameterization (CITY), with a maximum effect over Paris grid point. An evaluation is proposed in the next section by comparison with observation time series available in Paris area.

3.3 Impacts of urban modeling at the local scale with Paris as case study

Paris urban climate and urban heat island are investigated by comparing ALADIN-Climate outputs with homogenized long-term time series presented in Sect. 2.2.2.

3.3.1 Comparison of T_{min} and T_{max} distributions

The daily probability distribution functions of T_{min} and T_{max} are calculated from both observations and ALADIN-Climate outputs for urban (Fig. 9a) and rural (Fig. 9b) areas. The dashed line indicates the mean of observation distribution. In addition, the biases between experiments and observations related to the mean of distributions are presented in Table 6.

As expected, the three experiments give comparable results for rural temperature since the surface data are very little modified from one simulation to another. The comparison between observed and modeled distributions shows that the general shape of distributions is correctly reproduced by
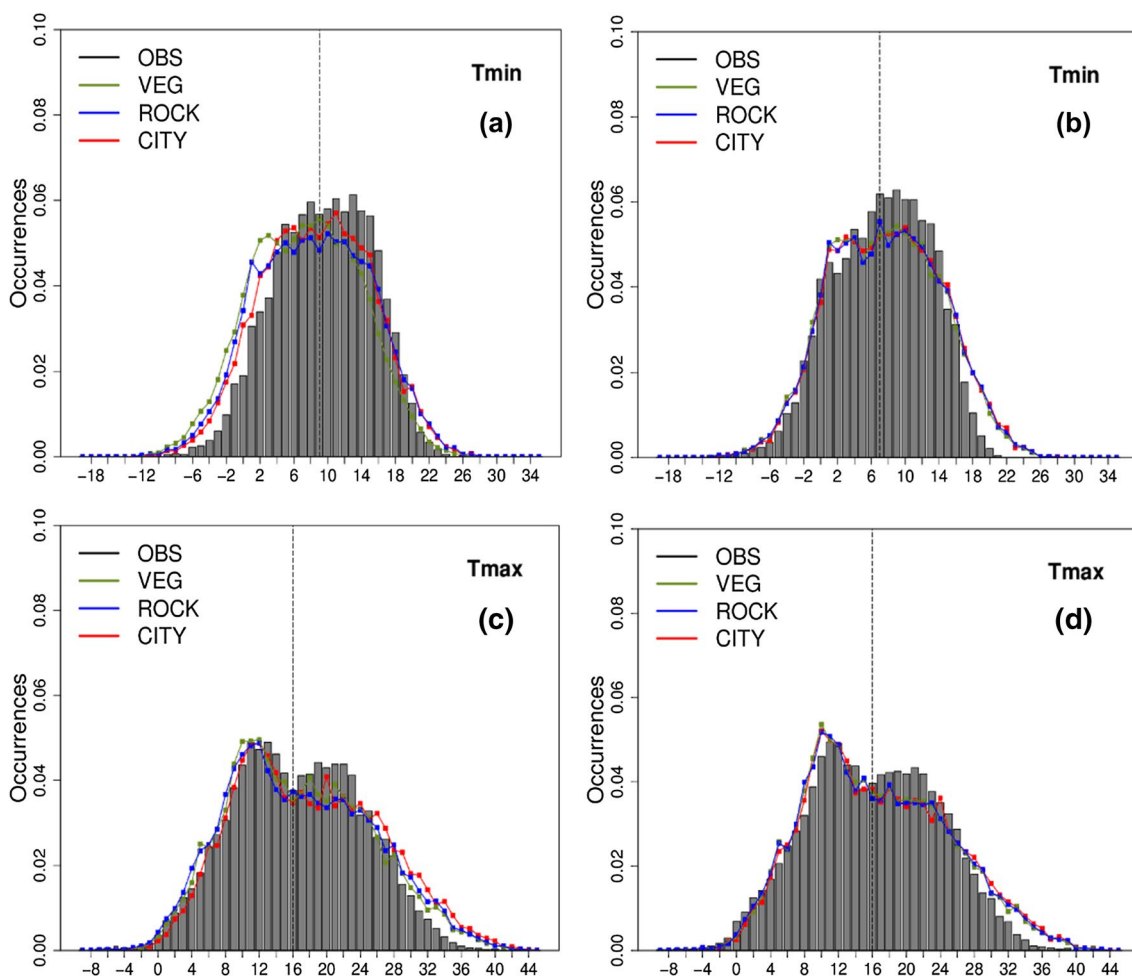

Fig. 9 Distribution of daily minimum (top) and maximum (bottom) temperatures in the city center (**a, c**) and in rural areas (**b, d**)

Table 6 Anomalies of mean temperatures compared to observations (Montsouris station data for the urban reference temperature; the average of Chartres and Melun stations data for the rural reference temperature)

	Urban			Rural		
	VEG	ROCK	CITY	VEG	ROCK	CITY
ΔT_{min} (°C)	− 2.0	− 1.0	− 0.7	+ 0.3	+ 0.5	+ 0.5
ΔT_{max} (°C)	+ 0.3	+ 0.4	+ 1.4	+ 0.5	+ 0.5	+ 0.8

the model for both T_{min} and T_{max} even though the secondary maximum is smaller in the model for T_{max}. In adequacy with the warm biases previously noticed for summer condition in Sect. 3.1.3, a slight overestimation by 0.5 °C of distribution means is observed (Table 6). This is mainly explained by an overestimation of warm extremes in T_{min} and T_{max} distributions (see Fig. 9).

For urban temperature, the comparison of distribution means between observations and ROCK indicates biases of − 1.0 °C for T_{min} and + 0.4 °C for T_{max} (Table 6), respectively related to an underestimation of cold extremes for T_{min} and an overestimation of warm extremes for T_{max} (Fig. 9a). Some differences are noticed between VEG, ROCK, and CITY T_{min} and T_{max} distributions. The CITY T_{min} distribution is in better agreement with observations than VEG and ROCK. For T_{max} distributions, all experiments indicate an overestimation of the warmest temperatures, with a greater bias for CITY. These points are discussed in the next section through urban heat island analysis.

It also has to be noticed that the double gaussian shape of observed T_{max} distributions is uncommon and could be associated with weather regimes or seasonal atmospheric conditions. However, this required deeper analyses that are beyond the scope of this study.

3.3.2 Comparison of UHI distributions

Figure 10a, b compares the observed and modeled distributions of nighttime and daytime UHI intensities. In case of CITY, the TEB and ISBA models calculate distinct air temperatures for the urban and natural parts of the grid cell, so that the UHI can be computed in two ways: by using as urban temperature the average temperature of the grid cell (Turb), or by using the TEB air temperature only (Turb$_{TEB}$). Both distributions of UHI are referred to as CITY and CITY(TEB), respectively. In order to evaluate objectively the distributions, a coefficient (hereafter referred to as 'Shared' and expressed as a fraction of the OBS distribution area) is calculated as the intersection area between each of modeled-UHI distributions and the OBS distribution. A coefficient of 1 means that the two distributions are identical while a coefficient of 0 means that the two distributions are entirely disjointed. The mean, the standard deviation, the skewness (i.e. third standardized moment, that measures the asymmetry of the distribution), and the 99th quantile associated to each distribution are also presented in Fig. 11a, b.

At night, almost the entire OBS distribution is positive which translates to a daily occurrence of UHI in Paris with an mean intensity of + 2.1 °C. The distribution however covers a wide range of values with a standard deviation of 1.3 °C and a 99th quantile up to 5.3 °C. In addition, one can
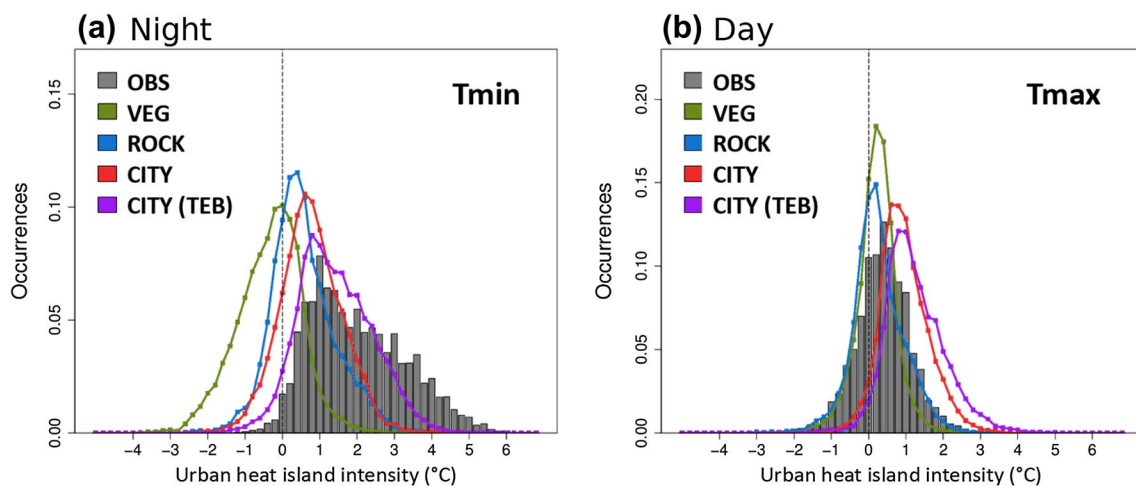
Fig. 10 Distribution of nocturnal (left) and diurnal (right) UHIs
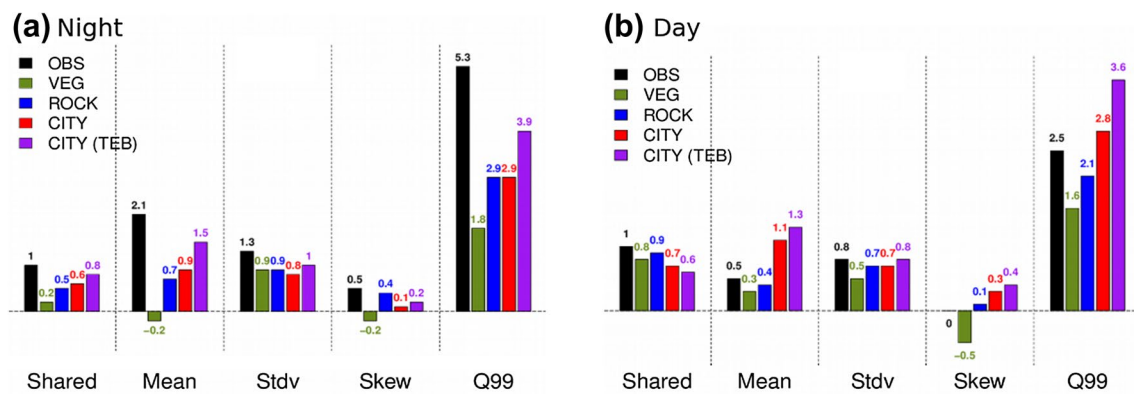
Fig. 11 Statistical scores associated to nocturnal (left) and diurnal (right) UHIs. Shared is defined as the area of intersection between an experiment distribution and the observed distribution. Stdv, Skew and Q99 correspond to the standard deviation, the skewness coefficient and the 99th quantile

note a strong left-side asymmetry highlighted by a skewness coefficient below 1. During the day, the OBS distribution is symmetric (skewness of 0) and centered on its mean value (0.5 °C) with a standard deviation of 0.8 °C and a low 99th quantile of 2.3 °C.

In comparison, the VEG distribution is zero-centred since urban areas are replaced by natural cover. ROCK underestimates UHI intensity and misses the warmer part of the distribution. It also overestimates the cases of negative UHIs. These defects are also noticed, in a lesser extent, for CITY distribution. They are likely to be explained by the low model horizontal resolution which smooths morphological urban parameters (by spatial interpolation) and understimates urban fabric compactness for inner city of Paris. CITY and CITY(TEB) nonetheless provide the most realistic distributions. They intersect 60 and 80%, respectively, of the observation one (against 20 and 50% only for VEG and ROCK). The distribution averages i.e. 0.9 °C for CITY and 1.5 °C for CITY(TEB) are also more comparable to the 2.1 °C obtained for observations. In addition, CITY(TEB) better fit with observations for the lowest values, but also by increasing the occurrence of intense UHIs with a 99th quantile of 3.9 °C.

During the day (see Fig. 10b), VEG misses the extreme positive UHIs. ROCK matches the observation for both extreme positive and negative UHIs, while CITY and CITY(TEB) overestimate UHIs. The vegetation surrounding the Montsouris public park station contributes to mitigate the local air temperature (and consequently the UHI effect) by evapotranspiration during daytime. This process is probably underestimated by the model, that could explain the shift of modeled UHI distribution. In addition, the overestimation of incoming solar radiation by ALADIN-Climate (Sect. 3.1.2) leads to a near-surface atmosphere warming that is amplified in urban areas due to great heating capacities of impervious surfaces.

3.3.3 Comparison of modeled surface energy fluxes

The surface energy balance (SEB) modeled in the city center is analyzed in order to better understand why the urban canopy model gives on average more intense UHIs during the day. Table 7 summarizes for each experiment the surface energy fluxes simulated at daytime (model outputs at 12 UTC), i.e. the source term that is net radiation (RN), and the sink sources that are sensible heat flux (H), latent heat flux (LE), and storage heat flux (G). These sink terms are also expressed as percentages of absorbed energy in order to evaluate and compare the partitioning between experiments. The Bowen ratio calculated as the ratio between H and LE is another way to characterize the SEB.

As expected, the Bowen ratio is lower than 1 for VEG because the SEB for natural covers gives latent heat fluxes higher than sensible heat fluxes. In ROCK, the lower vegetation fraction produces less evapotranspiration and then less latent heat flux (-6% compare to VEG). In response, the sensible heat flux slightly increases, but especially the storage heat flux ($+5\%$) because the dynamical roughness length over rocks is weak which limits the turbulent fluxes. In CITY, the sensible heat flux increases by $+19\%$ while the latent heat flux (-17%) and the storage heat flux (-2%) are reduced. In this case, the surface exchanges are amplified by the city roughness (1.54 m for CITY against 0.13 m for ROCK, see Table 2). The storage heat flux is rather low because the urban parameters used for TEB correspond to a low urban compactness which favors the sensible heat exchanges (Bowen ratio goes up to 2.49). As a result, the differences of average UHI intensities are explained in the city center by the large sensible heat flux that leads to warmer near-surface temperature for CITY.

4 Conclusions

The new ALADIN-Climate version 6 has been coupled to SURFEX and run at a 12-km horizontal resolution over the France metropolitan area. It has been compared with the SAFRAN analyses data and evaluated for the four seasons independently. The precipitation bias does not exceed ± 0.5 mm day^{-1}, and T_{min} and T_{max} are correctly simulated with acceptable biases ranges comparing to previous studies. The main defect of the model is the lack of cloudiness leading to too high incoming solar radiation and resulting in a T_{max} overstimation with a positive bias of 2.8 °C.

ALADIN-Climate has then be used to perform a sensitivity analysis on three different representations of urban areas: CITY corresponding to explicit description and modeling of cities with a specific urban parameterization, ROCK that is the conventional approach of ALADIN-climate model describing impervious urban covers as rock, and VEG for which cities are replaced by natural covers. This analysis showed that, even for a spatial resolution of 12 km, urban areas have an impact on modeling near-surface temperature. In particular, it has been shown that cities can influence their surrounding at a regional scale. By comparison with the VEG experiment, the French largest cities all induce a warming effect for near-surface temperature. This warming is maximum for Paris (up to 1.5 °C for summer T_{min}) which is much more urbanized and populated than other French cities and covers 65% of the corresponding cell of ALADIN-Climate 12-km resolution grid. Moreover, the intensity and the spatial extent of the cities influence was found to be greater when using a detailed urban canopy model than for the ROCK experiment.

Finally, based on long-term time series, the Paris urban heat island has been evaluated for each experiment. It remains tricky to very accurately evaluate the modeled air temperature in urban environment, with data provided by operational network stations that are located in open areas (most of the time in urban parks). Nonetheless it was found that the explicit resolution of urban processes through an urban canopy model improves the nighttime UHI modeling. The next ALADIN-Climate simulations could consequently be done by activating the TEB model (within the SURFEX platform) as it does not result in an extra numerical cost. A bias persists in daytime air temperature modeling. This overestimation seems to be more related to the overestimation of incoming solar radiation in ALADIN-Climate simulations than to the TEB parameterization itself.

These results highlight the gain brought by a detailed urban parameterization for regional climate models. Such a configuration would make possible to simulate scenarios of global adaptation strategies (greening, air-conditioning, urban planning scenarios) to climate change and to assess their benefits at the regional scale. Nonetheless, in order to study more accurately urban planning scenarios, the 12-km horizontal resolution remains a limitation. Dynamical downscaling approaches are currently studied and tested to reach 2.5-km horizontal resolutions over large urban areas. Eventually, this study underlines the interest and need for sensitivity analyses and inter-comparison projects on surface parameterizations.

Appendix 1

Ecoclimap II consists in 273 land cover classes, with the specificity of including 11 urban classes, that are "dense urban areas", "mediterranean suburban areas", "temperate suburban areas", "cold suburban areas", "industrial and commercial areas", "railways networks", "port facilities", "airport", "mines and construction sites", "urban parks", "sport facilities". Each urban class is described as a fraction of impervious covers (road and buildings composing the urban canyons) and a fraction of natural covers. As an example, "temperate suburban areas" which is largely present in France are composed of 40% of natural land surface (grass and trees), 30% of impervious ground-based surfaces and 30% of buildings. If the urban model is activated, impervious surfaces are dealt with TEB, whereas natural land surfaces are dealt with ISBA. Without explicit modeling of cities, the impervious covers are converted in natural land surfaces to be dealt by ISBA.

The Ecoclimap II classification is projected on ALADIN-Climate simulation grid, so that each mesh consists in a combination of land covers. The parameters associated to each land cover class (as defined in Ecoclimap II database) are aggregated over the mesh according to respective cover fractions. The tile fractions of sea, inland water, natural land surface and urban areas can be derived, as well as input data required by the surface models.

Figure 12 illustrates for the three ALADIN-Climate scenarios the methodology that has been applied to compute the cover fractions of natural and urban tiles for each model grid cell, starting from the fractions of land cover classes provided by Ecoclimap II. For this example, the grid cell is composed of urban areas (cover A that is a combination of gardens, roads, and buildings) and natural land surface (cover B that is a combination of two different vegetation types Veg1 and Veg2).
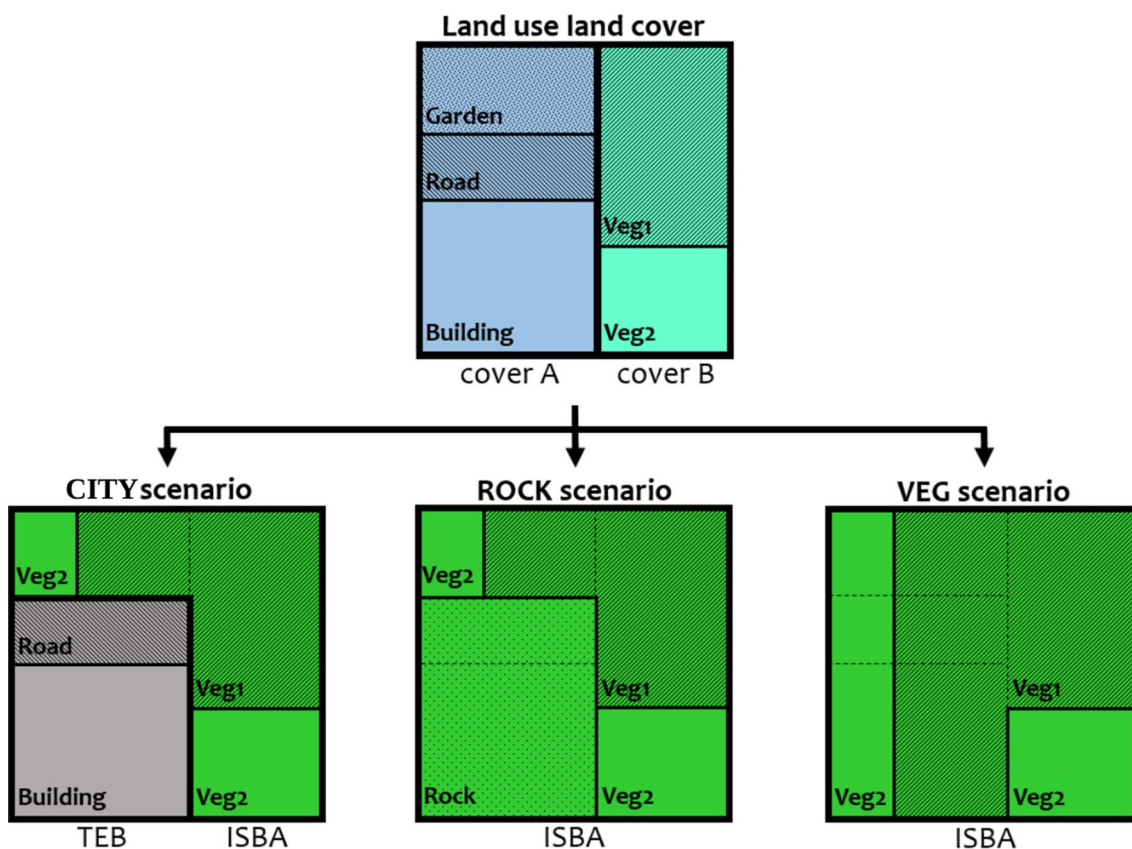
Fig. 12 Example of land use treatment in SURFEX for each experiments

For the CITY experiment where urban areas are explicitly modeled with TEB, building and road fractions represent the urban tile, whereas the garden fraction is part of the natural tile. To do so, this garden fraction is merged with Veg1 and Veg2 by keeping constant the ratio between Veg1 and Veg2. For the ROCK experiment that is the regular ALADIN-Climate configuration (Colin et al. 2010), urban areas are entirely converted in natural land surfaces: the impervious part (road and buildings) is converted to rocks while the garden part is merged with Veg1 and Veg2 (as described previously, respecting the partition between Veg1 and Veg2). For the VEG experiment, all urban areas are replaced by their surrounding vegetation. The fraction of urban cover A in Fig. 12 is removed and the natural cover B fills up the grid cell. This step is performed by maintaining the ratio between Veg1 and Veg2 constant.

Appendix 2

It was mention in Sect. 3.2.2 that the Regional Effect Index (REI) coefficient has been calculated in order to be comparable with Trusilova et al. (2007) works. This coefficient

allows to evaluate the spatial extend of the potential impact of urbanized areas on air temperature. It is expressed as:

$$REI(x) = \frac{A_{rur_{aff}}(x) + A_{urb}}{A_{urb}}$$

where x is the T_{min} ot T_{max}, A_{urb} the urban area defined as the number of grid cells where the urban fraction is greater or equal to 10%, and $A_{rur_{aff}}(x)$ the non urban area (i.e. cells where urban fraction is less than 10%) affected by a significant temperature difference. In this study, the significance is defined by a Student test carried out on the VEG experiment and with a threshold value set at 90%. However, this coefficient is dependent on both the significance test and the urban fraction threshold that defined the urban area.

The significance test is used to set a threshold below which the magnitude of differences can be neglected. This test can be statistical for instance based on the Student test, or global i.e. based on a unique reference temperature difference for each grid cell. In this discussion, three tests have been carried out: two identical Student test (Test A and Test B) with different threshold values set at 90 and 95% respectively, and a global test (Test C) for which a minimum
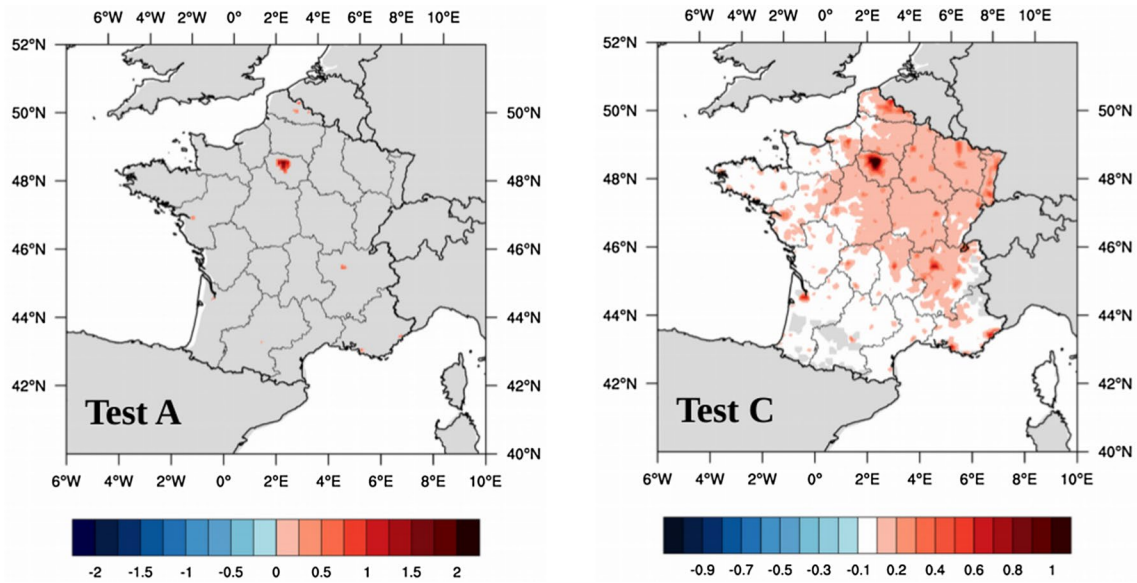
Fig. 13 Differences of minimal temperatures (in °C) for JJA between CITY and VEG. Pixels used for REI calculation are shown in warm colors

Table 7 Distribution in W m^{-2} (%) of net radiation (RN) between storage (G), sensible heat (H) and latent heat (LE) fluxes and Bowen ratio (Bo) associated at 12 UTC

	Surface energy budget components at 12 UTC (Paris)				
	RN	**H**	**LE**	**G**	**Bo (−)**
VEG	300	116 (39%)	124 (41%)	60 (20%)	0.94
ROCK	303	121 (40%)	106 (35%)	77 (25%)	1.14
CITY	289	177 (59%)	71 (23%)	53 (18%)	2.49

Table 8 Regional Effect Index for three difference significant tests and three different urban areas

	Test A		Test B		Test C	
	T_{min}	T_{max}	T_{min}	T_{max}	T_{min}	T_{max}
Ftown > 5%	1.07	1.05	1.00	1.00	19.3	40.1
Ftown > 10%	1.29	1.17	1.02	1.00	27.1	56.4
Ftown > 15%	1.80	1.43	1.18	1.03	40.0	83.3

Test A and Test B: Student tests with threshold set a 90 and 95% respectively. Test C: significant threshold for temperate differences set at 0.1 °C

temperature difference has been fixed at 0.1 °C. This test is performed with the thought that a temperature difference lower that 0.1 °C may not be percieved by the human body. Results are presented in Table 8 for minimal and maximal temperatures and illustrated in Fig. 13 for minimal temperature. Note that in Fig. 13, Test B is not shown since no regional impact was found (REI of 1.0).

Three different urban fraction thresholds have also been used. Indeed, in REI coefficient, the urban area should includes all the grid cells that are more affected by their own urban component than by the surrounding grid cells. However, since a pixel-to-pixel evaluation does not seem relevant nor standard, a global test on the urban fraction is applied over the whole domain. The sensitivity of REI has thus been tested on three urban fraction (Ftown) thresholds set at 5, 10 and 15%. Results are presented in Table 8 for the three significance tests.

Except for T_{min} with an urban fraction threshold of 15%, Test B does not indicate any urban impact on surroundings, contrary to Test A which indicates urban impacts on both T_{min} and T_{max}. Test C is more permissive and highlights a major impact of cities on the regional climate. With this test, REI grows up to 56.4. In addition, contrary to Test A and Test B, Test C reveals a impact twice greater for T_{max} than T_{min}. This enhance the needs for a standard test based both on one hand on a robust statistical approach and on another hand on human body perception. Eventually, if one wants to keep a statistical test, a Student test with a threshold value set at 70% would also lead to a higher REI for T_{max} (4.1) than for T_{min} (2.6).

Looking now at the difference of REI according to the urban fraction threshold, one can note that, as expected, both for T_{min} and T_{max} and whatever the significance test considered, REI values increase with the threshold. However, it is important to note that even with a low threshold of 5%, Test A and Test C found a significant impact of the cities on their surrounding.

References

Abdel-Lathif AY, Roehrig R, Beau I, Douville H (2018) Single-column modeling of convection during the CINDY2011/DYNAMO field campaign with the CNRM climate model version 6. J Adv Model Earth Syst. https://doi.org/10.1002/2017MS001077

Alkama R, Decharme B, Douville H, Becker M, Cazenave A, Sheffield J, Voldoire A, Tyteca S, Le Moigne P (2010) Global evaluation of the ISBA–TRIP continental hydrological system. Part I: comparison to GRACE terrestrial water storage estimates and in situ river discharges. J Hydrometeorol 11(3):583–600

Bador M, Terray L, Boé J, Somot S, Alias A, Gibelin A-L, Dubuisson B (2017) Future summer mega-heatwave and record-breaking temperatures in a warmer France climate. ERL. https://doi.org/10.1088/1748-9326/aa751c

Batjes NH (2009) Harmonized soil profile data for applications at global and continental scales: updates to the WISE database. Soil Use Manag 25(2):124–127

Belamari S, Pirani A (2007). Validation of the optimal heat and momentum fluxes using the ORCA2LIM global oceanice model. In: Marine environment and security for the European area Integrated Project (MERSEA IP), deliverable D4, p 88

Bénichou P, Le Breton O (1987) Prise en compte de la topographie pour la cartographie des champs pluviométriques statistiques (Incorporating topography in statistical mapping of precipitation fields, in French. La Météorologie 19:23–34

Bougeault P, Lacarrere P (1989) Parameterization of orography-induced turbulence in a mesobeta-scale model. Mon Weather Rev 117(8):1872–1890

Charnock H (1955) Wind stress on a water surface. Q J R Meteorol Soc 81(350):639–640

Christensen JH, Boberg F, Christensen OB, Lucas-Picher P (2008) On the need for bias correction of regional climate change projections of temperature and precipitation. Geophys Res Lett 35(20):L20709

Colin J, Déqué M, Radu R, Somot S (2010) Sensitivity study of heavy precipitation in limited area model climate simulations: influence of the size of the domain and the use of the spectral nudging technique. Tellus A 62(5):591–604

Cubasch U, Hasselmann K, Höck H, Maier-Reimer E, Mikolajewicz U, Santer BD, Sausen R (1992) Time-dependent greenhouse warming computations with a coupled ocean-atmosphere model. Clim Dyn 8(2):55–69

Cuxart J, Bougeault P, Redelsperger JL (2000) A turbulence scheme allowing for mesoscale and large-eddy simulations. Q J R Meteorol Soc 126(562):1–30

Decharme B, Douville H (2006) Introduction of a sub-grid hydrology in the ISBA land surface model. Clim Dyn 26:65–78

Decharme B, Douville H (2007) Global validation of the ISBA sub-grid hydrology. Clim Dyn 29:21–37

Dee DP, Uppala SM, Simmons AJ, Berrisford P, Poli P, Kobayashi S et al (2011) The ERA-Interim reanalysis: configuration and performance of the data assimilation system. Q J R Meteorol Soc 137(656):553–597

Durand Y, Brun E, Merindol L, Guyomarch G, Lesaffre B, Martin E (1993) A meteorological estimation of relevant parameters for snow models. Ann Glaciol 18(1):65–71

Durand Y, Giraud G, Brun E, Mérindol L, Martin E (1999) A computer-based system simulating snowpack structures as a tool for regional avalanche forecasting. J Glaciol 45(151):469–484

EEA (2005) Sustainable use and management of natural resources. European Environment Agency, Denmark

Faroux S, Kaptué Tchuenté AT, Roujean JL, Masson V, Martin E, Moigne PL (2013) ECOCLIMAP-II/Europe: a twofold database of ecosystems and surface parameters at 1 km resolution based on

satellite information for use in land surface, meteorological and climate models. Geosci Model Dev 6(2):563–582

Fouquart Y, Bonnel B (1980) Computations of solar heating of the earth's atmosphere- A new parameterization. Beitraege zur Physik der Atmosphaere 53:35–62

Früh B, Becker P, Deutschländer T, Hessel JD, Kossmann M, Mieskes I et al (2011) Estimation of climate-change impacts on the urban heat load using an urban climate model and regional climate projections. J Appl Meteorol Climatol 50(1):167–184

Giorgi F (1990) Simulation of regional climate using a limited area model nested in a general circulation model. J Clim 3(9):941–963

Giorgi F, Jones C, Asrar GR (2009) Addressing climate information needs at the regional level: the CORDEX framework. WMO Bull 58(3):175

Guérémy JF (2011) A continuous buoyancy based convection scheme: one-and three-dimensional validation. Tellus A 63(4):687–706

Hamdi R, Van de Vyver H, Termonia P (2012) New cloud and microphysics parameterisation for use in high-resolution dynamical downscaling: application for summer extreme temperature over Belgium. Int J Climatol 32(13):2051–2065

Hamdi R, Van deVyver H, De Troch R, Termonia P (2014) Assessment of three dynamical urban climate downscaling methods: Brussels's future urban heat island under an A1B emission scenario. Int J Climatol 34(4):978–999

Houghton JT, Ding YDJG., Griggs DJ, Noguer M, van der Linden PJ, Dai X et al (2001) Climate change 2001: the scientific basis. The Press Syndicate of the University of Cambridge, Cambridge

Hua LJ, Ma ZG, Guo WD (2008) The impact of urbanization on air temperature across China. Theor Appl Climatol 93(3–4):179–194

Jacob D, Petersen J, Eggert B, Alias A, Christensen OB, Bouwer LM et al (2014) EURO-CORDEX: new high-resolution climate change projections for European impact research. Reg Environ Chang 14(2):563–578

Jones PD, Lister DH, Li Q (2008) Urbanization effects in large-scale temperature records, with an emphasis on China. J Geophys Res Atmos 113:D16

Kjellström E, Nikulin G, Strandberg G, Christensen OB, Jacob D, Keuler K, Lenderink G, van Meijgaard E, Schär C, Somot S, Sorland SL, Teichmann C, Vautard R (2018) European climate change at global mean temperature increases of 1.5 and 2 °C above pre-industrial conditions as simulated by the EURO-CORDEX regional climate models. Earth Syst Dynam 9:459–478

Kusaka H, Masayuki HARA., Takane Y (2012) Urban climate projection by the WRF model at 3-km horizontal grid increment: dynamical downscaling and predicting heat stress in the 2070's August for Tokyo, Osaka, and Nagoya metropolises. J Meteorol Soc Jpn Ser II 90:47–63

Lamptey BL, Barron EJ, Pollard D (2005) Impacts of agriculture and urbanization on the climate of the Northeastern United States. Glob Planet Chang 49(3):203–221

Leduc M, Laprise R (2009) Regional climate model sensitivity to domain size. Clim Dyn 32(6):833–854

Lemonsu A, Kounkou-Arnaud R, Desplat J, Salagnac JL, Masson V (2013) Evolution of the Parisian urban climate under a global changing climate. Clim Chang 116(3–4):679–692

Lopez P (2002) Implementation and validation of a new prognostic large-scale cloud and precipitation scheme for climate and data-assimilation purposes. Q J R Meteorol Soc 128(579):229–257

Masson V (2000) A physically-based scheme for the urban energy budget in atmospheric models. Bound Layer Meteorol 94(3):357–397

Masson V, Le Moigne P, Martin E, Faroux S, Alias A, Alkama R et al (2013) The SURFEXv7. 2 land and ocean surface platform for coupled or offline simulation of earth surface variables and fluxes. Geosci Model Dev 6:929–960

McCarthy MP, Harpham C, Goodess CM, Jones PD (2012) Simulating climate change in UK cities using a regional climate model, HadRM3. Int J Climatol 32(12):1875–1888

Mestre O, Domonkos P, Picard F, Auer I, Robin S, Lebarbier E et al (2013) HOMER: a homogenization software—methods and applications. Időjárás 117(1):47–67

Mlawer EJ, Taubman SJ, Brown PD, Iacono MJ, Clough SA (1997) Radiative transfer for inhomogeneous atmospheres: RRTM, a validated correlated-k model for the longwave. J Geophys Res Atmos 102(D14):16663–16682

Morcrette J, Barker H, Cole J, Iacono M, Pincus R (2008) Impact of a new radiation package, McRad, in the ECMWF integrated forecasting system. Mon Weather Rev 136(12):4773–4798

Nabat P, Somot S, Mallet M, Chiapello I, Morcrette J-J, Solmon F, Szopa S, Dulac F, Collins W, Ghan S, Horowitz LW, Lamarque JF, Lee YH, Naik V, Nagashima T, Shindell D, Skeie R (2013) A 4-D climatology (1979–2009) of the monthly tropospheric aerosol optical depth distribution over the Mediterranean region from a comparative evaluation and blending of remote sensing and model products. Atmos Meas Tech 6:1287–1314

Nabat P, Somot S, Mallet M, Sanchez-Lorenzo A, Wild M (2014) Contribution of anthropogenic sulfate aerosols to the changing Euro-Mediterranean climate since 1980. Geophys Res Lett 41(15):5605–5611

Nabat P, Somot S, Mallet M, Sevault F, Chiacchio M, Wild M (2015) Direct and semi-direct aerosol radiative effect on the Mediterranean climate variability using a coupled regional climate system model. Clim Dyn 44:1127–1155

Nikulin G, Lennard C, Dosio A. Kjellström E, Chen Y, Hänsler A, Kupiainen M, Laprise R, Mariotti L, Fox Maule C, van Meijgaard E, Panitz H-J, Scinocca JF, Somot S (2018) The effects of 1.5 and 2 degrees of global warming on Africa in the CORDEX ensemble. Environ Res Lett. https://doi.org/10.1088/1748-9326/aab1b1

Noilhan J, Mahfouf JF (1996) The ISBA land surface parameterisation scheme. Glob Planet Chang 13(1–4):145–159

Oke TR (1982) The energetic basis of the urban heat island. Q J R Soc Meteorol Soc 108(455):1–24

Oke TR (1987) The urban energy balance. Progress Phys Geogr 12(4):471–508

Piriou JM, Redelsperger JL, Geleyn JF, Lafore JP, Guichard F (2007) An approach for convective parameterization with memory: separating microphysics and transport in grid-scale equations. J Atmos Sci 64(11):4127–4139

Prein AF, Gobiet A, Truhetz H, Keuler K, Goergen K, Teichmann C et al (2015) Precipitation in the EURO-CORDEX simulations: high resolution, high benefits? Clim Dyn 46(1–2):383–412

Quintana-Segui P, Le Moigne P, Durand Y, Martin E, Habets F, Baillon M et al (2008) Analysis of near-surface atmospheric variables: validation of the SAFRAN analysis over France. J Appl Meteorol Climatol 47(1):92–107

Ricard J, Royer J (1993) A statistical cloud scheme for use in an AGCM. Ann Geophys 11:1095–1115

Stone B (2007) Urban and rural temperature trends in proximity to large US cities: 1951–2000. Int J Climatol 27(13):1801–1807

Tramblay Y, Ruelland D, Somot S, Bouaicha R, Servat E (2013) High-resolution Med-CORDEX regional climate model simulations for hydrological impact studies: a first evaluation of the ALADIN-climate model in Morocco. Hydrol Earth Syst Sci 17:3721–3739. https://doi.org/10.5194/hess-17-3721-2013

Trusilova K, Jung M, Churkina G, Karstens U, Heimann M, Claussen M (2007) Urbanization impacts on the climate in Europe: numerical experiments by the PSU–NCAR mesoscale model (MM5). J Appl Meteorol Climatol 47(5):1442–1455

Vautard R, Gobiet A, Jacob D, Belda M, Colette A, Déqué M et al (2013) The simulation of European heat waves from an ensemble of regional climate models within the EURO-CORDEX project. Clim Dyn 41(9–10):2555–2575

Vidal JP, Martin E, Franchistéguy L, Baillon M, Soubeyroux JM (2010) A 50-year high-resolution atmospheric reanalysis over France with the Safran system. Int J Climatol 30(11):1627–1644

Voldoire A, Sanchez-Gomez E, y Mélia DS, Decharme B, Cassou C, Sénési S et al (2013) The CNRM-CM5. 1 global climate model: description and basic evaluation. Clim Dyn 40(9–10):2091–2121

Watson L, Michou M, Nabat P, Saint-Martin D (2017) Assessment of CNRM coupled ocean-atmosphere model sensitivity to the representation of aerosols. Clim Dyn. https://doi.org/10.1007/s00382-017-4054-6

Yang Z, Dominguez F, Gupta H, Zeng X, Norman L (2016) Urban effects on regional climate: a case study in the phoenix and tucson "sun corridor". Earth Interact 20(20):1–25